Exact analytical solutions and corresponding Monte Carlo models for the problem of light transport in turbid media with smooth absorption and discrete scattering at the single scattering approximation

Andrey P. Tarasov [a,b*], Saydulla Persheyev [c], Dmitry A. Rogatkin [a]

[a]*Moscow Regional Research and Clinical Institute named after M.F. Vladimirsky, Shchepkina str. 61/2, 129110, Moscow, Russia*

[b]*Shubnikov Institute of Crystallography of Federal Scientific Research Centre "Crystallography and Photonics" of Russian Academy of Sciences, Leninskiy Prospekt 59, 119333, Moscow, Russia*

[c]*School of Physics and Astronomy, St Andrews University, KY16 9SS, St Andrews, The United Kingdom of Great Britain and Northern Ireland*

[*]E-mail address: tarandrew17@gmail.com (A.P. Tarasov)

Abstract

In spite of the radiative transport theory is widely used in various problems of biomedical optics, ocean optics, optics of atmosphere, etc., there are few light transport problems that can been solved analytically. Therefore, Monte Carlo (MC) numerical simulations are used in the majority of practical applications. In this work, the problem of light transport in continuously absorbing and discrete scattering media for the pencil-like incident beam was considered theoretically at the single scattering approximation. The strict and closed-form analytical solutions of the problem were derived and compared with MC numerical results. Two sets of probabilistic parameters for the MC algorithm were explored. The first one was the classical set for continuous absorbing and smooth scattering media, while the second one was the newly substantiated set for continuous absorbing and discrete scattering media corresponding to the analytical medium's model used. It was shown, that if the same model is used in the MC simulations and the analytical approach, all results are identical. The divergence up to 10% between obtained analytics and MC results for the case of continuous absorption and smooth scattering was observed.

Keywords: light transport; discrete scattering; biological tissue; analytical solution; single scattering; Monte Carlo

1. Introduction

The radiative transport theory (RTT) is widely used today in biomedical optics, radiation heat transfer, ocean optics, optics of atmosphere, etc. [1-7]. In spite of the problems of light scattering in turbid media can also be considered with the use of Maxwell's formalism methods [6,8], the photometric RTT using the classical radiative transport equation (RTE) [1,2] remains the more convenient and usable technique for many practical applications since the electrodynamic approach is more complex, requires additional statistical tools, and is often far from accurate and frequently needed closed-form analytical solutions [2,9]. However, in the general case of a turbid medium with absorption and a phase scattering function of any kind, the closed-form analytical solution of the RTE is not known either. There is only a limited number of problems, which have been solved analytically: the well-known Milne problem and its

rigorous solution by Chandrasekhar [1,10], diffusion equations [11], Kubelka-Munk model [2,12] if to consider it as a 1D light transport problem approximation, etc. All of them have a limited applicability, therefore most practical problems are solved today with the use of well-developed Monte Carlo (MC) numerical simulations [3,4,9].

In general, the classical RTT, including aforementioned analytical models and the vast majority of numerical MC models, uses the approach of smooth scattering and continuous absorption media, when the scattering coefficient μ_s is introduced as a somewhat analogue to the absorption coefficient μ_a [13]. Also a set of discrete both absorbing and scattering particles are often considered as a turbid media [7]. However, for a number of practical applications the case of continuous absorption and discrete scattering media should be taken into account. One of these problems is the light propagation in living tissues, where cell membranes as well as tissue layers are actually discrete light scatterers inside a smooth absorbing medium. Recently the generally improved two-flux Kubelka-Munk approach which gives the exact and closed-form analytical solution of the one-dimensional (1D) multiple scattering problem for turbid media with smooth absorption and discrete scattering was published [14]. It was shown that there is a divergence between the results for the medium with continuous absorption and smooth scattering and the medium with continuous absorption with discrete scattering. Therefore, it is important to study this divergence in details from both methodical and fundamental (theoretical) points of view.

In this study, we explore the general RTE approach for the continuous absorption and discrete scattering model of light transport on the examples of the pencil-like beam illumination of weakly scattering media, for which the single scattering approximation (SSA) can be applied [7]. Indeed, the SSA has a limited application for the majority of real turbid media. Nevertheless, it is sometimes used in atmospheric and ocean optics, infrared optics, tissue optics, etc. [2,5,7,15-18], so it is also of a practical interest. What is more important, SSA for a pencil-like beam illumination, as it is shown in this article, facilitates obtaining the exact and closed-form analytical solution of the general RTE for any spatial cases.

We only consider stationary, time-independent energetic (photometric) problems, because it is exactly the fundamentals of the RTT phenomenology [14,19]. It means that we deal with the concepts of the pure ray theory describing light beams in terms of its power or energy, without taking into account both wave and quantum nature of the optical radiation, as it was initially proposed in the photometric RTT. We also do not take into consideration any boundary effects like boundary reflection or refraction due to the lack of their influence on the final comparison results for the smooth scattering and continuous absorption model, also called as classical model in this paper, and for the model of smooth absorption and discrete scattering.

Since the problems, which are more habitual to us, are mainly of a biomedical nature, all tasks in this study are adapted to light propagation in turbid biological tissues and medical diagnostic problems as we see them. In particular, for biomedical diagnostic purposes we often deal with the boundary values of light fluxes that can be registered by a photodetector placed on the frontal surface (illuminated surface) of tissue. Therefore, backscattered radiation escaping the medium is of our main interest in this study. Nevertheless, all other radiation inside the medium as well as transmitted through the medium can also be accurately estimated analytically with the use of the proposed approach.

To verify our analytical results we used MC numerical simulations. First, for the MC algorithm we used classical probabilistic parameters determined the for continuous absorbing

and smooth scattering turbid medium. In addition, because the MC with classical probabilistic parameters showed a slight discrepancy with the exact analytical results, we found how to modify MC parameters to accurately describe the discrete scattering case numerically. In both cases of MC modeling we employ a technique that operates with single photons. Being mathematically equivalent to sampling of photon packets [20,21] (the technique also known as the weighed photon model or the implicit capture) used in most contemporary MC simulations, this approach allows us to deal with absorption and scattering probabilities *ab initio*.

The paper is organized as follows. After this introduction, Section 2 describes the ideology of pencil-like beam propagation in the discrete scattering medium with continuous absorption. Sections 3 and 4 present derivations and comparisons for the 2D and 3D problems. In these two sections, where MC numerical results are used to describe the classical model, additionally, revised MC parameters and results for the discrete scattering case are presented. Section 5 discusses the obtained results and Section 6 gives the conclusions of the work.

2. Pencil-like incident beam propagation

The model representation of the pencil-like incident beam propagation inside the considered turbid medium is depicted in Fig. 2.1 (see also Refs. [14,19]). Such an illumination model is frequently used in the RTT [22] and in tissue optics, especially when modeling collimated laser irradiation [23]. In this pencil-like beam illuminating model, the incident δ-beam F_0 [W] penetrates a medium at the point $x = 0$ and propagates inside it as the 1D radiant flux $F_+(x)$ along the *X*-axis undergoing both scattering and absorption. In order to derive differential equations for $F_+(x)$, let us consider the transformation of the flux at the turbid interval Δx (by analogy with how it was done in Refs. [14,19]). As was mentioned in Introduction, the medium is supposed to be continuous light-absorbing, i.e. it has a continuous absorption coefficient μ_a [cm^{-1}] as in the classical approach, while scattering properties of the medium are determined by a number of discrete inhomogeneities (or simply scatterers, scattering centers) existing in the medium, each of which scatters a part R $(0 \le R < 1)$ of the flux $F_+(x)$ incident on it. In reality, scattering in the majority of real turbid media is not a continuous but a discrete process since it is due to light interaction with discrete inhomogeneities of the inner structure of the medium (such as cells' membranes in tissues, for example). Therefore, the proposed model of a turbid medium seems to be more adequate to reality than the model with smooth scattering.

Frequently, in the RTT such a discrete scattering approach is considered as "scattering on particles". However, there is a difference between light scattering on real dimensional particles and on discrete optical inhomogeneities inside a smooth absorbing substance. Furthermore, absorption of light inside a real particle can differ from the absorption of light outside the particle (inside a macro-homogenous substance containing the particles). We have no purpose to study any processes of light propagation and absorption inside particles, which is different from the conventional process of light absorption inside a continuous turbid substance. Moreover, the term "scattering particle" has a conditional meaning for the δ-beam $F_+(x)$ scattered due to the lack of any spatial dimensions of the beam. Therefore, our approach describes a certain idealized case. Our model of the turbid medium is close to living biological tissues where scattering inhomogeneities can be assumed to have no thickness, providing some kind of internal boundary scattering. This means that the scattering coefficient μ_s [cm^{-1}] must be additionally expressed analytically through the density of inhomogeneities μ_ρ [cm^{-1}] and a scattering factor R of a single inhomogeneity.

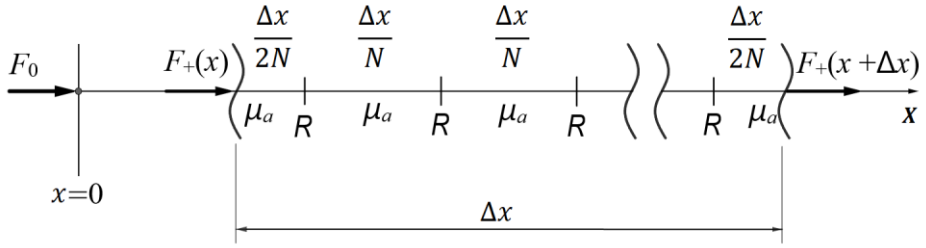

Fig. 2.1. Outline of the δ-beam $F_+(x)$ propagation and scattering problem illustrating the inner structure of the interval Δx.

In the frame of the single scattering approximation (SSA) considered, it is assumed that the forward incident flux $F_+(x)$ inside a turbid medium undergoes both absorption and scattering, while the scattered radiation (a radiance L, see below) can only be absorbed along its way of propagation. Also, we do not take into consideration any external boundary effects, for example, external boundary reflections, due to the lack of their influence on the explored difference between smooth scattering and discrete scattering problem formulations. Thus, in our pencil-like incident beam model at SSA, the only process that should be considered as scattering is the scattering of δ-beam $F_+(x)$ on infinitesimal inhomogeneities (scatterers) distributed along the X-axis inside a smooth light-absorbing substance (the discrete scattering center approximation).

Let the small interval Δx of the turbid medium contain N equally-spaced inhomogeneities with spacing between them $\Delta x/N$. Distances from the first and the last inhomogeneities to the corresponding nearest boundary of Δx are $\Delta x/2N$ (Fig. 2.1). All intervals between the inhomogeneities have the same absorption coefficient μ_a. Such a geometry simplifies the derivation of the final analytical equations, but does not violate generality. It can be easily shown that a random distribution of distances between inhomogeneities with a certain average $\Delta x/N$ in the mean statistical sense will lead to the same result as for the proposed deterministic geometry.

Each of these infinitesimal scatterers inside Δx, like a point source of the scattered radiation, forms the spatially distributed radiant intensity $I(\theta,\varphi)$ [W·sr^{-1}], where θ is the polar angle between the direction of the flux $F_+(x)$ propagation and a new direction after the scattering event, and φ is the azimuthal scattering angle. Commonly, in the RTT the side scattering properties of turbid media with light scattering on particles is characterized by the scattering phase function (SPF) of a single scatterer $\rho(\theta,\varphi)$ [sr^{-1}] [3,7,9], so that $\rho(\theta,\varphi)$ determines $I(\theta,\varphi)$ as follows [8,24]:

$$I(\theta,\varphi) = F_0 \cdot \rho(\theta,\varphi)\,, \tag{2.1}$$

where F_0 is the incident flux [W] illuminating the scatterer.

In our study SPF $\rho(\theta,\varphi)$ is not a function of Cartesian coordinates of a scatterer's position inside the medium as it is for anisotropic media since all scatterers in our model are assumed to be equivalent (we consider the macro-isotropic medium). Thus, in our case, when we consider scatterers located along the X-axis, as well as the incident on them flux $F_+(x)$, it yields:

$$I(\theta,\varphi,x) = F_+(x) \cdot \rho(\theta,\varphi), \tag{2.2}$$

Also, in the RTT usually for scattering on particles in multidimensional spatial problems, SPF is determined as the normalized differential scattering cross section [25]. However, because our incident beam is infinitesimal in its width (δ-beam), all scatterers on its way are infinitesimal too. Therefore, SPF satisfies to the normalization condition:

$$\int_0^{4\pi} \rho(\theta,\varphi)d\Omega = R \tag{2.3}$$

with $d\Omega$ being the infinitesimal unit solid angle [sr^{-1}].

Such a condition Eq. (2.3), determining the part of the scattered radiation as equal to $R < 1$ (instead of $R = 1$ for the perfect scattering), accounts for "imperfection" of scattering by each inhomogeneity, because there is a part of radiation that goes through each inhomogeneity without any interaction forming a transmitted flux. It allows one to derive a differential equation for $F_+(x)$. By definition, its derivative is

$$\frac{dF_+(x)}{dx} = \lim_{\Delta x\to 0}\frac{\Delta F_+(x)}{\Delta x} = \lim_{\Delta x\to 0}\frac{F_+(x+\Delta x)-F_+(x)}{\Delta x}. \tag{2.4}$$

Considering partial scattering with $R < 1$ from each inhomogeneity and absorption with the absorption coefficient μ_a at intervals between them, we can write for $F_+(x+\Delta x)$:

$$F_+(x+\Delta x) = F_+(x)e^{-\mu_a\Delta x}(1-R)^N. \tag{2.5}$$

According to Refs. [14,19], the inhomogeneities density μ_ρ [cm^{-1}] is introduced by

$$\mu_\rho = \lim_{\Delta x\to 0}\frac{N}{\Delta x}. \tag{2.6}$$

The right part of Eq. (2.4) using Eq. (2.5) comes to

$$F_+(x)\lim_{\Delta x\to 0}\frac{e^{-\mu_a\Delta x}(1-R)^N-1}{\Delta x}, \tag{2.7}$$

and, hence, the differential equation for $F_+(x)$ is the well-known in RTT differential equation of the first-order:

$$\frac{dF_+(x)}{dx} = -(\mu_a+\mu_s)F_+(x), \tag{2.8}$$

where [14,19]

$$\mu_s = -\mu_\rho\ln(1-R) \tag{2.9}$$

is the scattering coefficient expressed through the density of inhomogeneities μ_ρ and R, as was required.

As can be seen, Eq. (2.8) is the known differential equation for $F_+(x)$ at SSA, which is indistinguishable in its structure from the analogous equation for a smooth scattering model [13]. However, the scattering coefficient represented by Eq. (2.9) differs from the conventional $\mu_s = \mu_\rho R$, intuitively introduced for a smooth scattering model by Ishimaru [2], and tends to it only for $R \ll 1$. Therefore, for not so small R all numerical results for discrete and smooth scattering models may differ.

In the classical RTT, the attenuation coefficient $\mu_t = \mu_a + \mu_s$ is also often introduced. However, in this study, it is convenient to use notations β_i for both attenuation and back (side-) scattering coefficients (see below) in order to match notations in the cited sources. Thus, we denote the attenuation coefficient as follows:

$$\beta_1^+ = \mu_a + \mu_s, \tag{2.10}$$

where superscript "+" identifies the attenuation of the forward flux $F_+(x)$.

The exact analytical solution of such a formulated problem for $F_+(x)$ is known, (e.g., Ref. [14]):

$$F_+(x) = F_0e^{-\beta_1^+x}. \tag{2.11}$$

Scattering of $F_+(x)$ inside such a turbid medium forms the scattered field of a radiance L, which needs to be determined. In next two sections, we explore the problem in both 2D and 3D spatial formulations. Indeed, a 3D approach is more real, but a 2D ("flatland") scattering model is more explicit and descriptive. Therefore, we start with the 2D problem treatment.

3. 2D problem

The outline of the 2D problem formulated is depicted in Fig. 3.1. The radiance L can be determined, for example, similarly as was proposed in Ref. [26], Eq. A1. There, the illuminating parallel light beam with an infinite diameter propagating inside an isotropic turbid medium in the positive direction and decreasing exponentially becomes a source of L. To describe the scattering process, a relative probability function of side scattering multiplied by a scattering coefficient is introduced as the side scattering characteristics of the turbid medium.

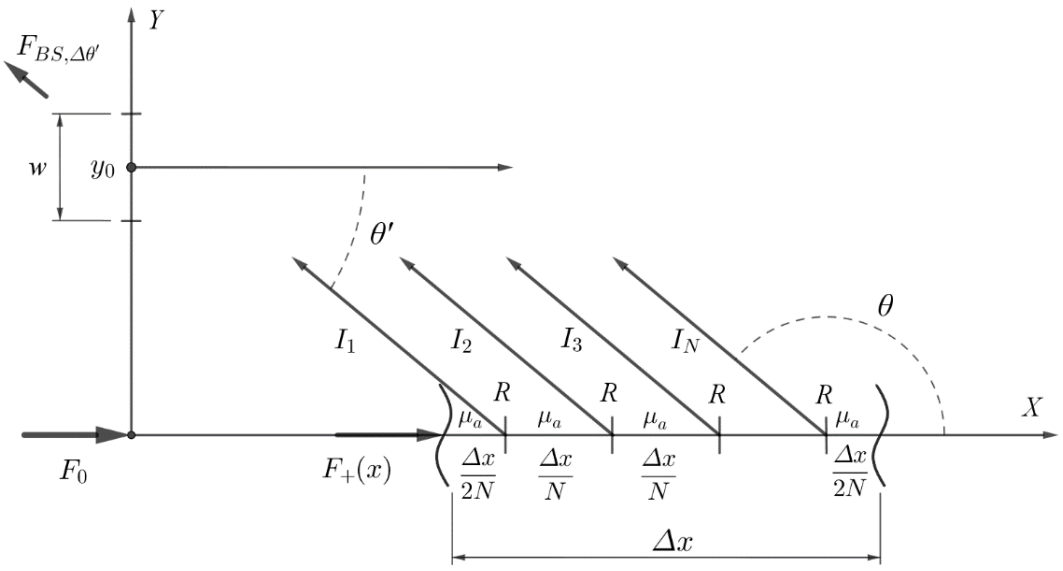

Fig. 3.1. Outline of the 2D scattering problem.

Let us consider a semi-infinite turbid medium. We need to find a part of radiation (a backscattered flux F_{BS}) escaping the medium through a photodetector's window placed on its frontal surface, which is a "line" in the 2D case [27]. The angular distribution of the scattered radiation inside 2D media can be described by the single planar angle θ [rad]. It means, that we need to solve the problem for backscattering angles $\theta \in \left(\frac{\pi}{2};\frac{3\pi}{2}\right)$. In addition, to find a flux in watts, the window's size [cm] should be given since the scattered field in the 2D case is a scalar field of the radiance $L_\theta(x,y)$ with the dimension [W·rad^{-1}·cm^{-1}] [27].

Let the pencil-like illuminating beam F_0 penetrates the 2D turbid medium at the point with coordinates $x = 0, y = 0$ (or (0,0)). For 2D SPF $\rho(\theta)$ [rad^{-1}] we can write from Eq. (2.2):

$$\rho(\theta) = \frac{I(\theta,x)}{F_+(x)}, \tag{3.1}$$

where $I(x,\theta)$ is the 2D radiant intensity with a dimension [W·rad^{-1}]. This SPF satisfies to the normalization condition $\int_0^{2\pi} \rho(\theta)d\theta = R$.

Using $I(\theta,x)$, we can now move on to finding the 2D radiance $L_\theta(x, y = 0)$ forming by the "turbid" element dx. By the definition [24,27]:

$$L_\sigma(x) = \frac{dI(\sigma,x)}{dx\cdot\cos(\sigma)}, \tag{3.2}$$

where σ is the angle between the observation direction and the external normal to dx.

After side scattering events at the angle θ inside dx, according to the RTT and SSA, we deal with the radiance $L_\theta(x,y)$ that propagates back to the *Y*-axis and is exposed to the absorbance only. It means that $L_\theta(x,y)$ obeys the 2D RTE in the form of the Beer-Lambert law:

$$\overrightarrow{l_\theta} \cdot grad L_\theta(x,y) = -\mu_a L_\theta(x,y), \tag{3.3}$$

where $L_\theta(x,y)$ is the radiance in the θ-direction at the point (x,y), $\overrightarrow{l_\theta} = \cos\theta\,\overrightarrow{e_x} + \sin\theta\,\overrightarrow{e_y}$ is the observation direction, $\overrightarrow{e_x}$ and $\overrightarrow{e_y}$ are the basis vectors, and factors multiplying them are the relevant direction cosines. Thus, we can write the system of differential equations (SDE) for the 2D problem as follows:

$$\begin{cases} \frac{dF_+(x)}{dx} = -\beta_1^+ F_+(x) \\ \cos\theta\,\frac{\partial L_\theta(x,y)}{\partial x} + \sin\theta\,\frac{\partial L_\theta(x,y)}{\partial y} = -\mu_a L_\theta(x,y) \end{cases}. \tag{3.4}$$

The solution of the 1st equation of the SDE (3.4) is Eq. (2.11). The general integral of the 2nd equation should be found in the form [28]

$$L_\theta(x,y) = e^{-\frac{\mu_a}{\sin\theta}y}\Phi(\sin\theta\cdot x - \cos\theta\cdot y). \tag{3.5}$$

Here $\Phi(\sin\theta\cdot x - \cos\theta\cdot y)$ is an arbitrary function with the argument $(\sin\theta\cdot x - \cos\theta\cdot y)$, which should be determined from a boundary condition. In our case, the boundary condition follows from a matching condition with the radiance $L_\theta(x,0)$ that is formed at the point $(x,0)$ as a result of scattering of $F_+(x)$ in the θ-direction (see Eqs. (2.2) and (3.2)). To derive $L_\theta(x,0)$ with the use of Eqs. (3.1) and (3.2), let us consider a set of discrete scattering events inside the interval Δx (Fig. 3.1) that produces a set of $I(\theta,x)$.

According to Eq. (2.2) and taking absorption into account, for the 1st inhomogeneity the radiant intensity can be expressed as follows:

$$I_1(\theta,\Delta x) = F_+(x)\rho(\theta)e^{-\mu_a\Delta x/2N}. \tag{3.6}$$

For the 2nd one,

$$I_2(\theta,\Delta x) = F_+(x)(1-R)\rho(\theta)e^{-\mu_a\Delta x/2N}e^{-\mu_a\Delta x/N} = I_1(\theta,\Delta x)e^{-\frac{\mu_a\Delta x}{N}}(1-R). \tag{3.7}$$

So, for the N^{th} scatterer we have

$$\begin{gathered} I_N(\theta,\Delta x) = F_+(x)(1-R)^{N-1}\rho(\theta)e^{-\frac{\mu_a\Delta x}{2N}}e^{-(\mu_a\Delta x/N)(N-1)} = \\ I_1(\theta,\Delta x)e^{-\mu_a\frac{\Delta x}{N}(N-1)}(1-R)^{N-1}. \end{gathered} \tag{3.8}$$

Summing all $I_i(\theta,\Delta x)$, we come to

$$\sum_{i=1}^{N} I_i\,(\theta,\Delta x) = F_+(x)\rho(\theta)\frac{e^{-\mu_a\Delta x/2N}\left[1-e^{-\mu_a\Delta x}(1-R)^N\right]}{1-(1-R)e^{-\mu_a\frac{\Delta x}{N}}}. \tag{3.9}$$

Taking into account Eq. (3.2), where $\sigma = \theta - \frac{\pi}{2}$ in our backscattering geometry, the radiance $L_\theta(x,y)$ at the point $(x,0)$, i.e. at any point of the *X*-axis, can be obtained as the limit:

$$L_\theta(x,0) = \frac{1}{\sin\theta}\lim_{\Delta x\to 0}\frac{\sum_{i=1}^{N} I_i(\Delta x)}{\Delta x} = F_+(x)\frac{\beta_2^+(\theta)}{\sin\theta} = F_0\frac{\beta_2^+(\theta)}{\sin\theta}e^{-\beta_1^+ x}, \tag{3.10}$$

where

$$\beta_2^+(\theta) = \rho(\theta)\frac{\beta_1^+ e^{-\frac{\mu_a}{2\mu_\rho}}}{1-e^{-\frac{\beta_1^+}{\mu_\rho}}} \tag{3.11}$$

is the side-scattering coefficient [rad^{-1}·cm^{-1}]. Note, only the single scatterer's SPF determines the dependence of SPF on θ in Eq. (3.11). Moreover, at $\mu_a \neq 0$ it differs from the classical $\beta_2^+(\theta) = \frac{\mu_s\cdot\rho(\theta)}{R}$ (see, e.g., Ref. [26], Eq. A1).

The described technique to obtain $\beta_2^+(\theta)$ was also used in Ref. [29] where the case of pure scattering without absorption was considered. The correctness of this technique was confirmed there by meeting the normalization condition $\int_0^{2\pi}\beta_2^+(\theta)d\theta = \mu_s$. In the limit of $\mu_a \to 0$, Eq. (3.11) gives the same normalization condition, therefore it is the more general case for $\beta_2^+(\theta)$ when absorption exists.

As the next step, basing on Eqs. (3.5) and (3.10), one can obtain

$$\Phi(\sin\theta\cdot x - \cos\theta\cdot y) = F_0\frac{\beta_2^+(\theta)}{\sin\theta}\exp\left[-\frac{\beta_1^+}{\sin\theta}(\sin\theta\cdot x - \cos\theta\cdot y)\right]. \quad (3.12)$$

Finally, $L_\theta(x,y)$ can be more conveniently written as

$$L_\theta(x,y) = F_0\frac{\beta_2^+(\theta)}{\sin\theta}\exp\left[-(\beta_1 x + \frac{\mu_a-\beta_1^+\cos\theta}{\sin\theta}y)\right]. \quad (3.13)$$

On the *Y*-axis, i.e. on the medium's frontal boundary, Eq. (3.13) takes the form

$$L_\theta(0,y) = F_0\frac{\beta_2^+(\theta)}{\sin\theta}\exp\left(-\frac{\mu_a-\beta_1^+\cos\theta}{\sin\theta}y\right). \quad (3.14)$$

The elementary flux on the medium's frontal boundary can be found from the radiance $L_\theta(0,y)$ by a definition [24,27] as follows:

$$dF_{\theta\prime}(0,y) = L_\theta(0,y)\cos\theta'\,d\theta' dy, \quad (3.15)$$

where θ' is the angle of the convergent radiation incidence on the *Y*-axis. Using Eq. (3.14) and taking into account that $\theta = \pi - \theta'$, an explicit form of Eq. (3.15) is as follows

$$dF_{\theta\prime}(0,y) = F_0\frac{\beta_2^+(\theta\prime)}{\tan\theta\prime}\exp\left(-\frac{\mu_a+\beta_1^+\cos\theta\prime}{\sin\theta\prime}y\right)d\theta' dy. \quad (3.16)$$

In order to have a possibility to compare the analytical result with MC numerical simulations, our theoretical aim here is to derive the backscattered radiant flux escaping the medium through the window of width *w* centered at the point $(0,y_0)$, and inside a small illuminating angle $\Delta\theta'$, which plays a role of a solid angle element in this 2D task.

The backscattered flux left the medium through a window centered at the point $(0,y_0)$ is only formed by the flux incident on the window. For simplicity, as previously mentioned, the boundary of the medium is considered here as refractive-index-matched and any beam refraction or reflection on the boundary is absent. Thus, its angular distribution can be obtained directly by the integration of Eq. (3.16) within the window's boundaries $y_1 = y_0 - \frac{w}{2}$, $y_2 = y_0 + \frac{w}{2}$:

$$\frac{dF_{BS}(0,y_0,\theta\prime)}{d\theta\prime} = F_0\frac{\beta_2^+(\theta\prime)}{\beta_1^+ + \frac{\mu_a}{\cos\theta\prime}}\left[\exp\left(-\frac{\mu_a+\beta_1^+\cos\theta\prime}{\sin\theta\prime}y_1\right) - \exp\left(-\frac{\mu_a+\beta_1^+\cos\theta\prime}{\sin\theta\prime}y_2\right)\right]. \quad (3.17)$$

Eq. (3.17) is valid for the case of $y_{1,2} \geq 0$. For $y_{1,2} \leq 0$, the similar expression can be obtained.

It is of interest to note that in the case of $\theta' = 0$ ($\theta = \pi$, i.e. strong backscattering), Eq. (3.17) comes to

$$\frac{dF_{BS}(0,0,0)}{d\theta'} = F_0\frac{\beta_2^+(0)}{2\mu_a+\mu_s}, \quad (3.18)$$

which corresponds to the expression for the 1D backscattered flux in Ref. [14]. Herein lies the connection between the known 1D [14] and our new 2D analytical solutions.

To check the correctness of the obtained analytical Eq. (3.17), one can compare its results with the numerical ones using the MC technique. In order to do this, we mainly need to find the flux

$$F_{BS,\Delta\theta'}(0,y_0,\theta') = \frac{dF_{BS}(0,y_0,\theta')}{d\theta'}\Delta\theta' \quad (3.19)$$

within a certain angular range $\Delta\theta'$, which is a finite element of the interval $(0;\frac{\pi}{2})$. This flux can be easily calculated with the use of (3.17). The total backscattered flux left the window in all

directions, if necessary, can be obtained then by the integration of Eq. (3.17) over θ' within the full range of $[0; \frac{\pi}{2}]$.

The classical (conventional) MC probabilistic parameters for 2D smooth scattering and continuous absorbing media at SSA should be listed as follows:

$$l_+^{cl} = -\frac{\ln \xi_1}{\mu_a+\mu_s},\ P_s^{cl} = \frac{\mu_s}{\mu_a+\mu_s},\ l_-^{cl} = -\frac{\ln \xi_2}{\mu_a},\ \theta = {D_\theta}^{-1}(\xi_3), \tag{3.20}$$

where ξ_i are the independent random numbers uniformly distributed within the range [0; 1], l_+^{cl} and l_-^{cl} are forward and backward pathlengths (for a photon propagating before and after the single scattering event correspondingly), P_s^{cl} is a scattering probability (superscript "*cl*" denotes "classical"), and θ is a scattering angle, which is calculated in MC according to its cumulative distribution function (CDF) D_θ. In terms used in the present paper, CDF is determined through the SPF as

$$\begin{aligned} D_\theta(\varepsilon) &= \frac{1}{R}\int_0^{k\varepsilon} \rho(\theta)d\theta, \\ D_\theta(\theta_1) &= \frac{1}{R}\int_0^{\theta_1} \rho(\theta)d\theta, \end{aligned} \tag{3.21}$$

where ε is a random number within $[0; 2\pi]$ and $k\varepsilon$ maps θ linearly. The dimensional constant $k = 1$ [rad] accounts for the dimension of SPF [rad^{-1}].

The comparison of the analytical solution (3.17)-(3.19) and corresponding MC results based on probabilistic parameters (3.20) for different window positions y_0 is shown in Fig. 3.2. In these examples we used $\rho(\theta) = \frac{R}{2\pi}$ (isotropic scattering) and $\rho(\theta) = \frac{3R}{8\pi}\left(1 + \frac{2}{3}\cos^2\theta\right)$ (Rayleigh-like scattering) for SPF. Due to a prolate shape of the Rayleigh-like SPF, the angular distribution of the backscattered flux in the case of Rayleigh-like scattering (Fig. 3.2b) is sharper, and the maximum is shifted towards $\theta' = 0$ as compared with the isotropic scattering case (Fig. 3.2a).

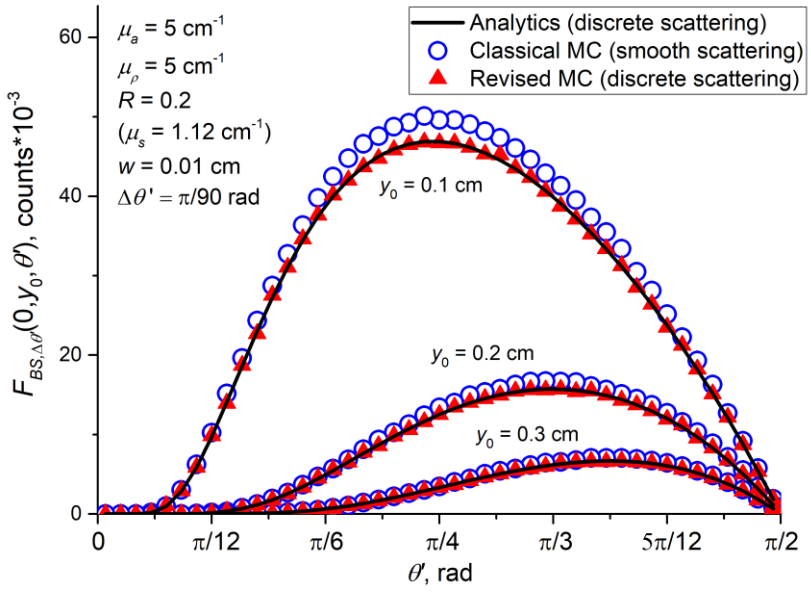

a

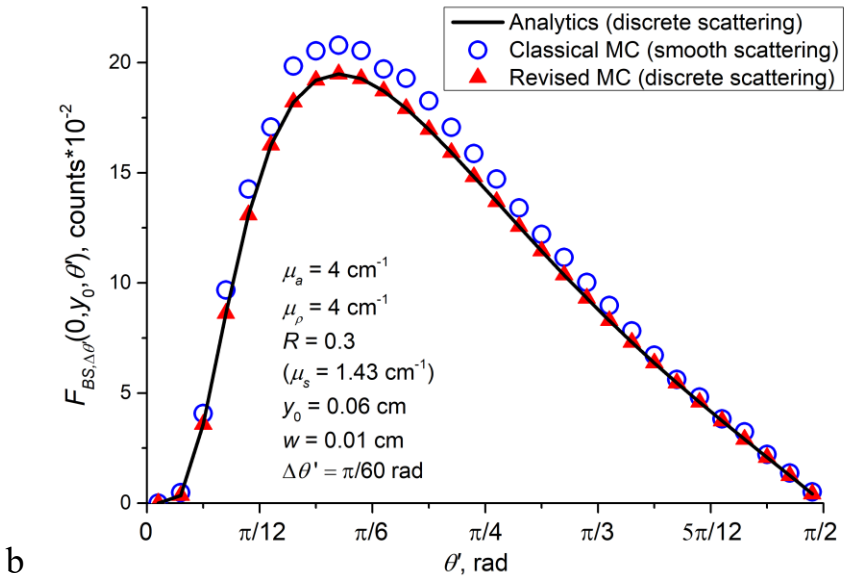

b

Fig. 3.2. Examples of the angular distribution of the backscattered flux calculated analytically by Eqs. (3.17)-(3.19) in comparison with results of the revised and classical MC models for different sets of parameters in the 2D case. SPF and a number of incident photons N_0 are: a) $\rho(\theta) = \frac{R}{2\pi}$, $N_0 = 5 \cdot 10^9$; b) $\rho(\theta) = \frac{3R}{8\pi}\left(1 + \frac{2}{3}\cos^2\theta\right)$, $N_0 = 40 \cdot 10^6$.

As can be seen from Fig. 3.2, the consideration of discrete scattering leads to the divergence of rigorous analytical results and numerical MC results computed with the use of probabilistic parameters for smooth scattering and continuous absorbing media. The relative divergence of two models calculated as the ratio of total backscattered fluxes (the integrals over the total polar angle range $[0; \frac{\pi}{2}]$) in cases of the classical MC model and the new analytical solution for discrete scattering for the example of the Fig. 3.2a is about 6 % for all window's positions y_0. Obviously, the reason of such a discrepancy lies in different approaches to accounting for scattering in a medium. Therefore, we can assume that if to modify the MC probabilistic parameters to account for discrete scattering rather than treating scattering as based on a homogeneous scattering coefficient, then the Monte Carlo method provides accurate solutions that agree with analytical solutions for that case.

Thus, basing on our analytics, we can propose how MC parameters should be modified to describe the discrete scattering case. Since at the transit from the smooth scattering model to the discrete scattering one at SSA the interaction mechanism formally does not change for photons of both propagation direction (attenuation for forward and backward photons are $\beta_1^+ = \mu_a + \mu_s$ and μ_a respectively), the pathlengths l_+^d and l_-^d (here superscript "d" means "discrete") remains the same as in Eq. (3.20). However, the scattering probability P_s^d is determined as the ratio of the fraction of the flux scattered by Δx to the fraction of the flux attenuated by Δx due to both scattering and absorption. Since the scattering process is characterized by $\beta_2^+(\theta)$, which is a function of both the scattering angle θ and SPF $\rho(\theta)$, the total fraction of the flux scattered by Δx in all directions is determined by the integration of $\beta_2^+(\theta)\Delta x$ over the range $[0; 2\pi]$. The fraction of the flux attenuated by Δx is $\beta_1^+\Delta x$. Thus, the scattering probability P_s^d must be determined as the ratio:

$$P_s^d = \frac{\int_0^{2\pi} \beta_2^+(\theta)d\theta}{\beta_1^+}. \qquad (3.22)$$

Within the discrete scattering center approximation, $\beta_2^+(\theta)$ is determined by Eq. (3.11), therefore Eq. (3.22) comes to:

$$P_s^d = \frac{e^{-\frac{\mu_a}{2\mu_\rho}}}{1-e^{-\frac{\beta_1^+}{\mu_\rho}}} \int_0^{2\pi} \rho(\theta) d\theta = \frac{Re^{-\frac{\mu_a}{2\mu_\rho}}}{1-e^{-\frac{\beta_1^+}{\mu_\rho}}}. \quad (3.23)$$

In order to build CDF $D_\theta(\varepsilon)$ for the scattering angle θ, we first define a function

$$S(\theta) = \frac{\int_0^\theta \beta_2^+(\theta_1) d\theta_1}{\int_0^{2\pi} \beta_2^+(\theta_1) d\theta_1} = \frac{\int_0^\theta \rho(\theta_1) d\theta_1}{\int_0^{2\pi} \rho(\theta_1) d\theta_1} \quad (3.24)$$

that determines the fraction of the incident flux $F_+(x)$ that is scattered in the angle range $[0;\theta]$, and then map the ranges of definition for the functions $S(\theta)$ and CDF $D_\theta(\varepsilon)$:

$$S(\theta) = D_\theta(\varepsilon). \quad (3.25)$$

Now, taking into account that the denominator in Eq. (3.24) equals R, we come to the expression for CDF that exactly repeats Eq. (3.21) and depends only on $\rho(\theta)$. However, when absorption exists, $\int_0^{2\pi} \beta_2^+(\theta) d\theta \neq \mu_s$ (see Eq. (3.11)). Thus, at SSA, probabilistic parameters for MC for two models differ by the scattering probability P_s, as was found earlier in the 1D case at multiple scattering [30]. Numerical results of MC modeling with the revised P_s^d (3.23) are also presented in Fig. 3.2. The total coincidence with the analytical solution is achieved using P_s^d.

4. 3D problem

Most terms and derivations in a 3D spatial case do not differ much from those introduced above for the 2D problem since in both our 2D and 3D model cases the incident flux propagates in the medium in a form of the infinitely narrow beam along *X*-axis and undergoes the same transformation into the scattered field. However, unlike the 2D problem, now we need to find a part of backscattered flux escaping a semi-infinite turbid medium through a photodetector's window, which is an "area" located at the *Y-Z* plane (Fig. 4.1), and the radiance L has a dimension [W·sr^{-1}·cm^{-2}]. The difference is also in the description of the 3D scattered field, which is now determined by two coordinate angles θ and φ instead of just θ in the 2D case. This effects on SPF that should be represented in these two spherical coordinates and should have the dimension of a reciprocal solid angle [sr^{-1}]. Keeping this in mind, in this section we will write 3D SPF in the azimuthal-independent form $\rho(\theta)$, which simplifies all equations and is commonly used in most studies. The normalization condition for such a 3D SPF is $\int_0^{4\pi} \rho(\theta) d\Omega = R$, similar to Eq. (2.3) with $d\Omega$ being the infinitesimal unit solid angle.

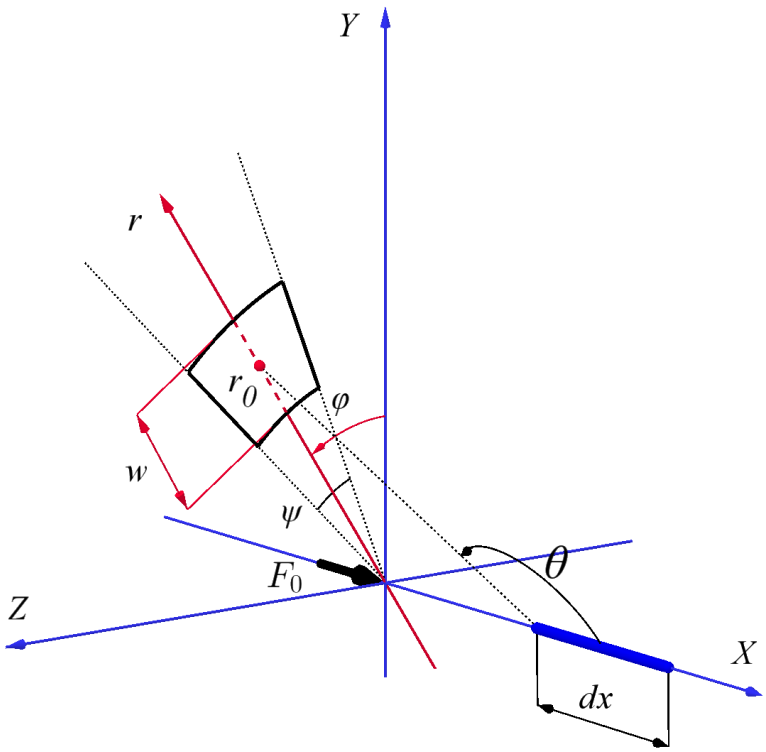

Fig. 4.1. Outline of the 3D scattering problem. The window is chosen in a shape of a ring sector with a width of w and a central angle of ψ in the polar coordinate system $\{r, \varphi\}$ (see the text for details).

The radiance $L_{\theta,\varphi}(x,y,z)$, which represents the scattered field in the 3D case, now propagates in the $\{\theta,\varphi\}$-direction given by the unit vector

$$\overrightarrow{e_{\theta,\varphi}} = \cos\theta\,\overrightarrow{e_x} + \sin\theta\cos\varphi\,\overrightarrow{e_y} + \sin\theta\sin\varphi\,\overrightarrow{e_z}. \tag{4.1}$$

Thus, the SDE for the 3D problem is

$$\begin{cases} \frac{dF_+(x)}{dx} = -\beta_1^+ F_+(x) \\ \cos\theta\frac{\partial L_{\theta,\varphi}(x,y,z)}{\partial x} + \sin\theta\cos\varphi\frac{\partial L_{\theta,\varphi}(x,y,z)}{\partial y} + \sin\theta\sin\varphi\frac{\partial L_{\theta,\varphi}(x,y,z)}{\partial z} = -\mu_a L_{\theta,\varphi}(x,y,z) \end{cases}, \tag{4.2}$$

where $L_{\theta,\varphi}(x,0,0)$ satisfies the boundary condition for the 2nd equation similar to Eq. (3.10). According to Ref. [28], the general solution of the 2nd equation of the SDE (4.2) can be found as

$$L_{\theta,\varphi}(x,y,z) = e^{-\frac{\mu_a}{\cos\theta}x}\Phi(\sin\theta\cos\varphi\cdot x - \cos\theta\cdot y, \sin\theta\sin\varphi\cdot x - \cos\theta\cdot z). \tag{4.3}$$

Similar to the 2D case, we obtain the function Φ and the radiance $L_{\theta,\varphi}(x,y,z)$ as follows:

$$\Phi(\sin\theta\cos\varphi\cdot x - \cos\theta\cdot y, \sin\theta\sin\varphi\cdot x - \cos\theta\cdot z) = F_0\frac{\beta_2^+(\theta)}{\sin\theta}\exp\left\{\frac{1}{\sin\theta}\left[\frac{\mu_a}{\cos\theta} - \beta_1^+\right]\left[(\sin\theta\cos\varphi\cdot x - \cos\theta\cdot y)\cos\varphi + (\sin\theta\sin\varphi\cdot x - \cos\theta\cdot z)\sin\varphi\right]\right\}; \tag{4.4}$$

$$L_{\theta,\varphi}(x,y,z) = F_0\frac{\beta_2^+(\theta)}{\sin\theta}\exp\left\{-\left[\beta_1^+ x + \frac{\mu_a - \beta_1^+\cos\theta}{\sin\theta}(y\cdot\cos\varphi + z\cdot\sin\varphi)\right]\right\}. \tag{4.5}$$

Note that Eq. (4.5) transforms to the 2D radiance Eq. (3.13) for $z = 0$ and $\varphi = 0$.

Due to specificity of the problem under consideration, where a source of scattered light in the 3D space is represented by, in fact, the 1D object (X-axis), scattered light fills the viewing solid angle $d\Omega'$ incompletely, making it degenerate (Fig. 4.2). In particular, this reflects on the

dimension of the radiance Eq. (4.5), which is [W·cm^{-1}·sr^{-1}]. Therefore, at the medium's boundary, i.e. in the *Y-Z* plane, the elementary flux should be written as

$$dF_{\theta',\varphi'}(0,y,z,\theta,\varphi) = L_{\theta,\varphi}(0,y,z)\cos\theta' \frac{d\Omega'}{l\sin\theta' d\varphi'} dS, \qquad (4.6)$$

where the factor $\frac{d\Omega'}{l\sin\theta' d\varphi'}$ represents the part of the solid angle filled with radiation (or the degenerate solid angle) and dS is the element of area in the *Y-Z* plane.

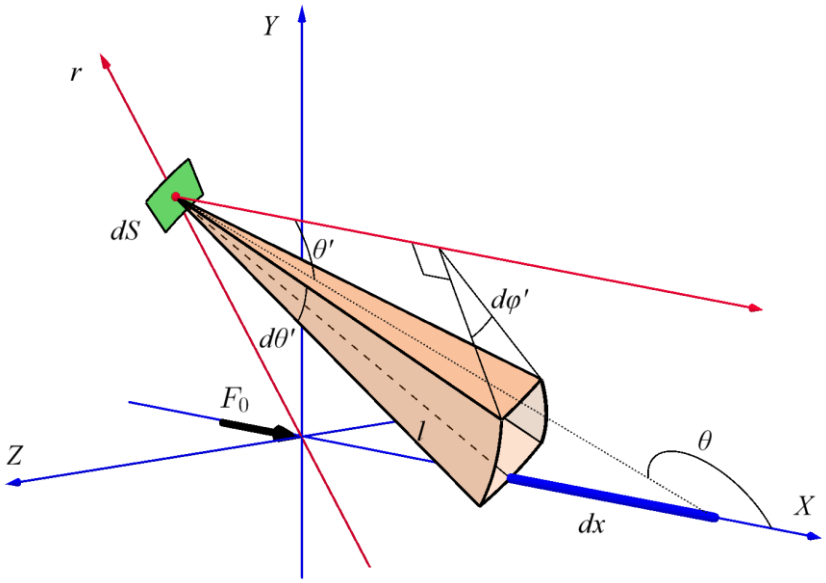

Fig. 4.2. The view of the radiating element *dx* from the point $(0, y, z)$.

Taking into account that $l = \frac{\sqrt{y^2+z^2}}{\sin\theta'}$ and $d\Omega' = \frac{\Omega_0}{k^2}\sin\theta'\, d\varphi' d\theta'$ (see Appendix A), Eq. (4.6) comes down to убрать $\frac{\Omega_0}{k^2}$ иначе придется вводить k в вырожденный телесный угол

$$dF_{\theta',\varphi'}(0,y,z) = \frac{L_{\theta,\varphi}(0,y,z)}{\sqrt{y^2+z^2}}\sin\theta'\cos\theta'\, d\theta' dS. \qquad (4.7)$$

Using Eq. (4.5) and taking into consideration that $\theta = \pi - \theta'$, we obtain

$$dF_{\theta',\varphi'}(0,y,z) =$$
$$F_0 \frac{\beta_2^+(\theta')}{\sqrt{y^2+z^2}} \exp\left\{-\frac{\mu_a+\beta_1^+\cos\theta'}{\sin\theta'}(y\cdot\cos\varphi + z\cdot\sin\varphi)\right\}\cos\theta'\, d\theta' dS. \qquad (4.8)$$

Prior to obtaining the backscattered flux, it is convenient to represent Eq. (4.8) in the polar coordinate system $\{r, \varphi\}$, where $r = \sqrt{y^2+z^2}$ (see Fig. 5.1). Then, $y = r\cos\varphi$, $z = r\sin\varphi$ and $dS = rdrd\varphi$. In this azimuthal-symmetric system, Eq. (4.8) takes the form of

$$dF_{\theta',\varphi'}(0,r) = F_0\beta_2^+(\theta')\exp\left\{-\frac{\mu_a+\beta_1^+\cos\theta'}{\sin\theta'}r\right\}\cos\theta'\, drd\theta' d\varphi, \qquad (4.9)$$

which is azimuthal-independent.

To calculate the angular distribution of the backscattered flux, one needs to integrate Eq. (4.9) over two variables: r and φ (and over $\theta' \in \left(0, \frac{\pi}{2}\right)$ if the total backscattered flux is of interest). In the common case of an arbitrary window $r = f(\varphi)$, the resulting integral may not be expressed in the explicit form. In order to compare these results with the similar MC output as simple as possible, and to make strict conclusions, we need to choose a detector's window of an appropriate shape. In the case of the considered azimuthal-symmetric problem, it is convenient to choose the window of the ring sector shape with a central angle ψ and a width w (see Fig. 4.1). The point $r = r_0$ is the end of the central radius of the ring. Upper and bottom boundaries of the

window are $r_1 = r_0 - \frac{w}{2}$ and $r_2 = r_0 + \frac{w}{2}$. With this choice, r does not depend on φ, and we can obtain the angular θ'-distribution of the backscattered flux left the window in the simple form:

$$\frac{dF_{BS}(0,r_0,\theta')}{d\theta'} = F_0 \frac{\beta_2^+(\theta')\sin\theta'}{\beta_1^+ + \frac{\mu_a}{\cos\theta'}} \left[e^{-\left(\frac{\mu_a+\beta_1^+\cos\theta'}{\sin\theta'}\right)r_1} - e^{-\left(\frac{\mu_a+\beta_1^+\cos\theta'}{\sin\theta'}\right)r_2} \right] \psi. \quad (4.10)$$

Here, one can see the analogy between Eqs. (4.10) and (3.17). Since the problem is considered in the azimuthal symmetry, the solution for the 3D problem can be actually obtained by "rotating" the 2D solution and taking into account the additional spatial dimension, which is accounted by the angle width ψ of the ring-shaped window and by $\sin\theta'$ in the numerator of Eq. (4.10). Wherein, actually $\sin\theta'$ is related to the sine in the expression for the solid angle element (see Appendix A), which plays the key role in the transition from the 2D consideration to the 3D one.

To compare MC results with this analytical one we need to find

$$F_{BS,\Delta\theta'}(0, r_0, \theta') = \frac{dF_{BS}(0,r_0,\theta')}{d\theta'} \Delta\theta', \quad (4.11)$$

where $\frac{dF_{BS}(0,r_0,\theta')}{d\theta'}$ is given by Eq. (4.10).

In 3D modeling, the set of classical 2D MC parameters (3.20) should be supplemented with $\varphi = {D_\varphi}^{-1}(\xi_4)$ for the azimuthal angle. To accurately describe the discrete scattering case, as it was proved in the previous section, MC simulation should be conducted with the revised for the discrete scattering case 3D scattering probability P_s^d. It can be found as follows:

$$P_s^d = \frac{\int_{4\pi}\beta_2^+(\theta)d\Omega}{\beta_1^+} = \frac{e^{-\frac{\mu_a}{2\mu\rho}}}{1-e^{-\frac{\beta_1^+}{\mu\rho}}} \int_{4\pi}\rho(\theta)d\Omega = \frac{Re^{-\frac{\mu_a}{2\mu\rho}}}{1-e^{-\frac{\beta_1^+}{\mu\rho}}}, \quad (4.12)$$

which turned out to be quantitatively the same as 2D P_s^d (3.23) within our approach.

Fig. 4.3 shows the comparison results computed for the cases of isotropic (Fig. 4.3a) and non-isotropic (Fig. 4.3b) scattering respectively. The case of the non-isotropic scattering is presented for the Henyey-Greenstein SPF. In addition, in Fig. 4.4 the dependence of the total backscattered flux on the window's position r_0 is presented for the same parameters as in Fig. 4.3a. Similarly to 2D problems, one can see that in the 3D case, there is a divergence (about 7% in Fig. 4.3a and Fig. 4.4, and about 10% in Fig. 4.3b) between the models caused by difference in the type of scattering under consideration.

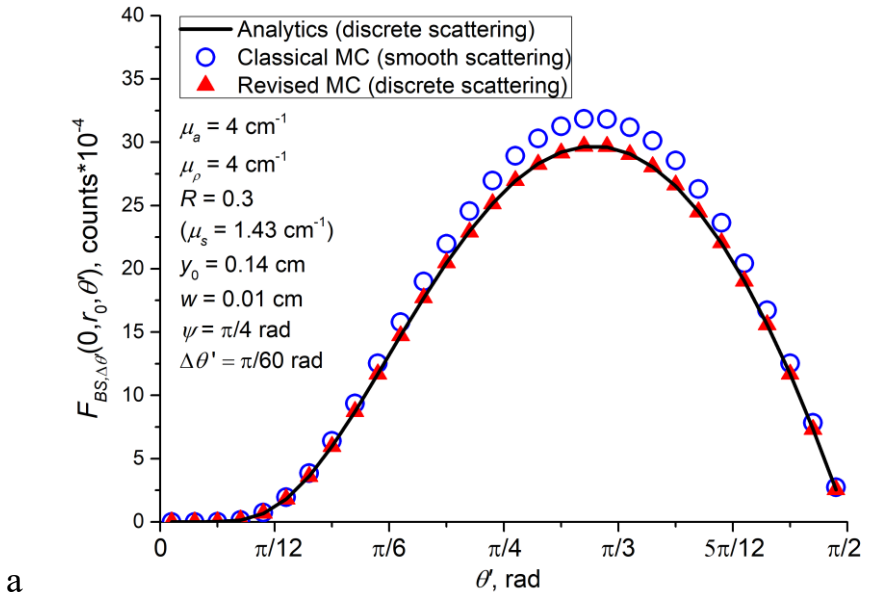

a

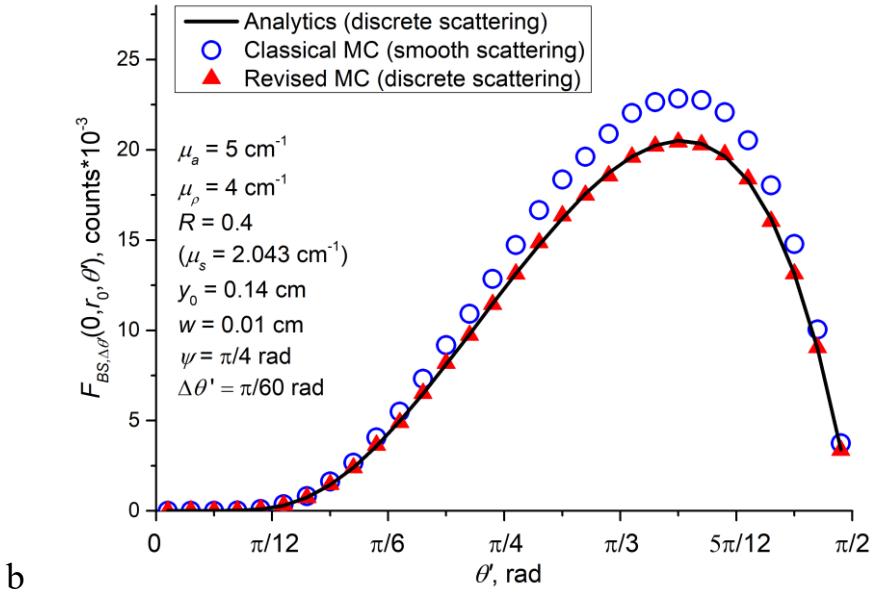

b

Fig. 4.3. Comparison of the analytical solution (4.10)-(4.11) for the 3D case of discrete scattering with the results of revised and classical MC models for different sets of optical properties of the medium. SPF and a number of incident photons N_0 are: a) $\rho(\theta) = \frac{R}{4\pi}$, $N_0 = 40 \cdot 10^9$; b) $\rho(\theta) = \frac{R}{4\pi}\frac{1-g^2}{(1+g^2-2g\cos\theta)^{3/2}}$ with $g = 0.9$, $N_0 = 60 \cdot 10^9$.

Also, as can be seen in Fig. 4.3, as well as in Fig. 3.2, while fluxes' magnitudes differ between the models, there is no shift of the maximums of its' angular distributions. It is a consequence of the fact that the revised probabilistic parameters both for 2D and 3D problems are different from the classical ones by the photon scattering probability P_s, which does not affect the scattering direction (CDFs remain the same).

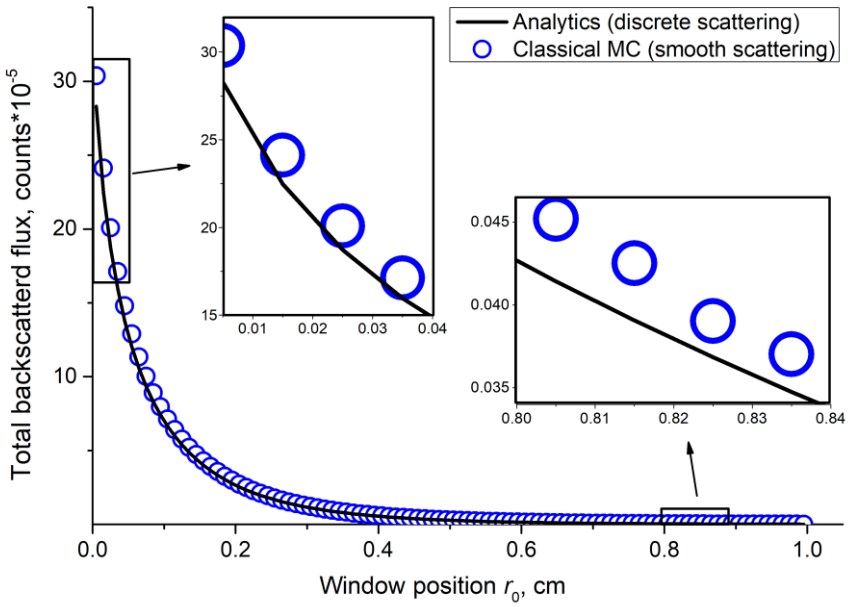

Fig. 4.4. The total backscattered flux as a function of the window's position r_0. Optical properties are taken as in Fig. 4.3a.

5. Discussion

In this work, we have theoretically studied 2D and 3D light transport problems for turbid media with discrete scattering and continuous absorption. One example of such media is biological tissues, which contain cell membranes and tissue layers as discrete optical inhomogeneities inside a smooth absorbing substance. Actually, scattering in the majority of real turbid media is not a continuous but a discrete process since it is due to the light interaction with discrete inhomogeneities of the inner structure of the medium. Therefore, the proposed model of a turbid medium seems to be more adequate to reality than the model with smooth scattering and continuous absorption, which is conventionally used in the radiative transport theory (RTT).

Indeed, we agree that our model of a turbid medium describes a quite idealized and limited case due to we additionally use the single scattering approximation (SSA) and the pencil-like beam illumination model. As a consequence, our scatterers in the model have no thickness and can be considered as infinitesimal scattering centers for the δ-beam propagating in the medium. However, to the best of our knowledge, there were not published analytical and closed form solutions of the light transport problem in 2D and/or 3D spatial cases for the problem considered. Therefore, we analytically solved the problem and compared our results with the numerical MC simulations.

In both spatial cases, the study has revealed the difference between obtained analytical results and MC numerical results if conventional (classical) probabilistic parameters for turbid media with smooth scattering and continuous absorption were used in the MC algorithm. Additionally, we have shown how these MC probabilistic parameters should be changed to precisely describe light propagation in a discrete scattering medium at SSA. If the same model is used in the MC simulations and the analytical approach, all results became identical. It confirms the correctness of the analytical solution for the theoretical model formulated.

The reason for the divergence between two models can be seen from the mathematical expression of the side-scattering coefficient β_2^+. This coefficient, derived in the SSA exactly

from “first principles” in our study, is not equal to μ_s used in the conventional RTT for a smooth scattering problem. In the MC model it is consistently manifested in the scattering probability P_s, which becomes unequal to the single scattering albedo $a = \mu_s/(\mu_a + \mu_s)$ phenomenologically accepted as P_s in the classical MC algorithm. Namely, the consideration of discrete scattering results in P_s (3.23) or (4.12), which is less than a in general. Thus, the use of classical $P_s^{cl} = a$ to numerically describe the light transport in discrete scattering media can provide overestimation as compared to the analytical result (or the revised MC model) specially obtained in our study for this particular case. The amplitude of the mentioned divergence depends on the relationship of optical properties of the medium. The divergence becomes much visible for the case when $\mu_a \gg \mu_s$ (or, more accurate, $\mu_a \gg \mu_\rho$ if to consider discrete scattering) or at least becomes comparable with μ_s – this is the case that is demonstrated in Figs. 3.2, 4.3, and 5.4. In the limit of $\mu_a \to 0$, the divergence tends to zero and the classical model with smooth scattering and continuous absorption can be used for all discrete scattering media. For example, this is a situation of light transport inside red or near infrared waveband through the tissue filled with blood, when μ_s can be several dozen times larger than μ_a. In such cases, the classical $P_s^{cl} = a$ undoubtedly can be used. However, already in green, blue or near ultraviolet spectral regions, where absorption by blood is much more intensive [31], it may be more expedient to use the discrete scattering model rather than the smooth scattering one.

It also should be noted that the divergence between classical and discrete scattering models concerns only the magnitude of the backscattered flux, not shifting the maximum of its angular distribution due to P_s does not affect the scattering direction (CDFs remain the same).

In this regard it is interesting to note that for the classical MC scattering probability $P_s^{cl} = a$, the corresponding 3D side-scattering coefficient $\beta_2^{+cl}(\theta)$ according to Eq. (4.12) should be written as follows:

$$\beta_2^{+cl}(\theta) = \mu_s \frac{\rho(\theta)}{R} \tag{5.1}$$

that is also in a good agreement with the classical analytics presented, for example, in Ref. [26], Eq. A1. Actually, Eq. (5.1) corresponds to the limit case of weak absorption ($\mu_a/\mu_\rho \ll 1$) for our $\beta_2^+(\theta)$ (3.11) if the normalization condition for 3D SPF is accepted as $\int_0^{4\pi} \rho(\theta) d\Omega = R$. Thus, rigorous solutions obtained in this work for discrete scattering media converge to the case of continuous scattering at $\mu_a/\mu_\rho \ll 1$ that confirms the correctness of our approach.

Though the SSA has a limited application for the majority of real turbid media, this approximation has great fundamental and methodological significance since it allows one to obtain accurate and closed-form analytical solutions. For example, using SSA in this study, we have succeeded to solve the problem of discrete scattering for 2D and 3D cases for the pencil-like incident beam. Meanwhile, for a multiple scattering case with discrete scattering, only 1D closed-form analytics [14] together with corresponding MC model [30] are known.

6. Conclusions.

We have considered the photometric problem of light transport in 2D and 3D turbid media in the single scattering approximation using the pencil-like beam illumination model. The turbid medium was supposed to be a composition of a continuous (smooth) light-absorbing substance and a set of discrete infinitesimal inhomogeneities (scatterers) inside it. Such a formulation of the problem allowed us to derive from the “first principles” all strict analytical and closed-form solutions for the backscattered fluxes left the medium through its frontal boundary.

All derived analytics was first compared to the conventional (classical) Monte Carlo (MC) numerical simulations dealing with continuously absorbing and smooth scattering media. It was shown that for some optical properties, particularly, when μ_a is comparable with μ_ρ, the divergence between models can be up to 10%. Meanwhile, in the limit of $\mu_a \to 0$, two models becomes equal.

Also, all derived analytics was compared to the revised MC model dealing with continuously absorbing, but discrete scattering media. In this case, both numerical and analytical results became identical, as well. On the one hand, this proves the correctness of the derivation of the presented analytics, but, on the other hand, it means that probabilistic parameters of the MC algorithm must always correspond to a tested analytical model and must be determined (must be known) explicitly.

Appendix A. Solid angle and its dimension. тогда это не надо

Common expression for a solid angle element is [24]

$$d\Omega = sin\,\theta\, d\varphi d\theta. \tag{A.1}$$

At first glance, the dimension of such a solid angle is [rad^2] [32]. However, in Eq. (A.1) some dimensional factors are missing. According to Ref. [8],

$$d\Omega = \Omega_0 \frac{dA}{l^2}, \tag{A.2}$$

where dA is the small area element of the sphere surface that is formed by the solid angle with a top in the center of the sphere of a radius l, $\Omega_0 = 1$ sr is a dimensional factor for the solid angle (Fig. A.1). The area element dA is calculated by multiplication of its sizes $dA = da \cdot db$.

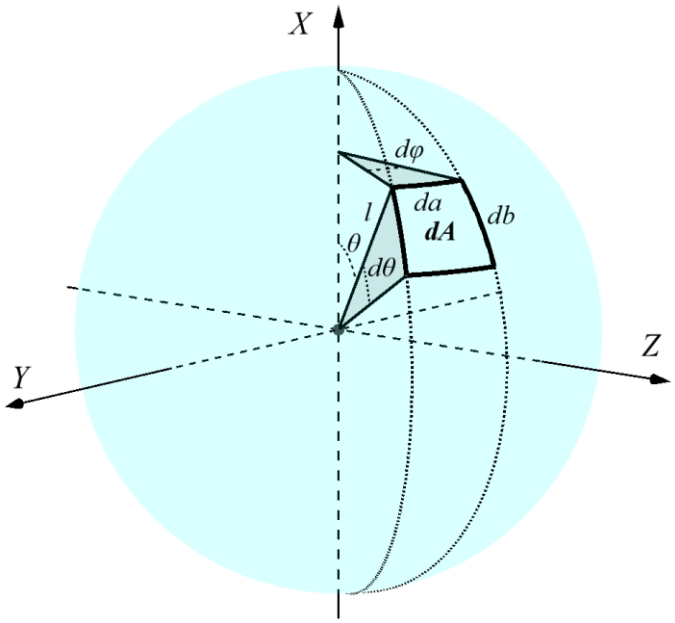

Fig. A.1. Determination of a solid angle.

Similar to Eq. (A.2), the element of the plane angle can be determined through the arc length and the circle radius as follows:

$$d\varphi = \varphi_0 \frac{da}{l \sin\theta}, \tag{A.3}$$

where $\varphi_0 = 1$ rad determines the plane angle dimension.

From this

$$da = l \sin\theta \frac{d\varphi}{\varphi_0}. \tag{A.4}$$

In the same manner, the size db is

$$db = l \frac{d\theta}{\theta_0}. \tag{A.5}$$

Denoting $\theta_0 = \varphi_0 = k$, we come to

$$d\Omega = \frac{\Omega_0}{k^2} sin\,\theta\, d\varphi d\theta \tag{A.6}$$

without any contradictions in the dimension.

References

1. Chandrasekhar S. Radiative transfer. New York: Dover Publications; 1960.
2. Ishimaru A. Wave propagation and scattering in random media. Piscataway: IEEE Press; 1997.
3. Tuchin VV, editor. Handbook of Optical Biomedical Diagnostics. 2nd ed. Vol. 1: Light-tissue interaction. Bellingham: SPIE Press; 2016.
4. Marchuk GI, Mikhailov GA, Nazareliev MA, Darbinjan RA, Kargin BA, Elepov BS. The Monte Carlo methods in atmospheric optics. Springer; 2013.
5. Spinrad RW, Carder KL, Perry MJ. Ocean optics. Oxford: Oxford University Press; 1994.
6. Mishchenko MI, Travis LD, Lacis AA. Multiple scattering of light by particles: radiative transfer and coherent backscattering. Cambridge University Press; 2006.
7. Kokhanovsky A., editor. Light Scattering Reviews. Single and Multiple Light Scattering. Springer Science & Business Media; 2006.
8. Rogatkin DA. Scattering of electromagnetic waves by a randomly rough surface as a boundary problem of laser radiation interaction with light-scattering materials and media. Opt Spectrosc (English Transl Opt i Spektrosk) 2004;97:455–63. https://doi.org/10.1134/1.1803651.
9. Meglinski I, Doronin A. Monte carlo modeling of photon migration for the needs of biomedical optics and biophotonics. Adv Biophotonics Tissue Opt Sect 2016:1–72. https://doi.org/10.1201/b15256-2.
10. Milne EA. Radiative equilibrium in the outer layers of a star: the temperature distribution and the law of darkening. Mon Not R Astron Soc 1921;81:361–75. https://doi.org/10.1093/mnras/81.5.361.
11. Wang LV, Wu HI. Biomedical optics: principles and imaging. John Wiley & Sons; 2012.
12. Kubelka P., Munk F. A contribution to the optics of paint. Z Tech Phys 1931;12:593-601.
13. Rybicki GB, Lightman AP. Radiative processes in astrophysics. Weinheim: Wiley-VCH; 2004.
14. Persheyev S, Rogatkin DA. A new look at fundamentals of the photometric light transport and scattering theory. Part 2: One-dimensional scattering with absorption. Her Bauman Moscow State Tech Univ Ser Nat Sci 2017;2017:65–78. https://doi.org/10.18698/1812-3368-2017-6-65-78.
15. Florescu L, Schotland JC, Markel VA. Single-scattering optical tomography. Phys Rev E - Stat Nonlinear, Soft Matter Phys 2009;79:1–10. https://doi.org/10.1103/PhysRevE.79.036607.
16. Kleinböhl A, Schofield JT, Abdou WA, Irwin PGJ, de Kok RJ. A single-scattering approximation for infrared radiative transfer in limb geometry in the Martian atmosphere. J Quant Spectrosc Radiat Transf 2011;112:1568–80. https://doi.org/10.1016/j.jqsrt.2011.03.006.
17. Schmitt JM, Knüttel A, Bonner RF. Measurement of optical properties of biological tissues by low-coherence reflectometry. Appl Opt 1993;32:6032. https://doi.org/10.1364/ao.32.006032.
18. Bonner R, Nossal R. Model for laser Doppler measurements of blood flow in tissue. Appl Opt 1981; 20:2097. https://doi.org/10.1364/ao.20.002097.

19. Persheyev S, Rogatkin DA. A new look at fundamentals of the photometric light transport and scattering theory. Part 1: One-dimensional pure scattering problems. Her Bauman Moscow State Tech Univ Ser Nat Sci 2017:79–94. https://doi.org/10.18698/1812-3368-2017-5-78-94.
20. Sobol' IM. The Monte Carlo Method. Chicago: The University of Chicago Press; 1974.
21. Tarasov AP, Rogatkin DA. Two Approaches in Monte Carlo Simulation of Laser Light Transport in Turbid Biological Media. 2020 Int. Conf. Laser Opt. (ICLO), 2020; pp. 1-1. https://doi.org/10.1109/ICLO48556.2020.9285703.
22. Zhang S, Wei W, Tan Z. Light diffusion in a turbid cylinder with an oblique incident pencil beam. J Opt Soc Am B 2018;35:909. https://doi.org/10.1364/josab.35.000909.
23. Webb CE, Jones JD, editors. Handbook of laser technology and applications. Bristol: Institute of Physics Publishing; 2004.
24. McCluney WR. Introduction to radiometry and photometry. 2nd ed. Norwood: Artech House; 2014.
25. Bohren CF, Huffman DR. Absorption and scattering of light by small particles. Weinheim: Wiley-VCH; 1998.
26. Star WM, Marijnissen JPA, Van Gemert MJC. Light dosimetry in optical phantoms and in tissues: I. Multiple flux and transport theory. Phys Med Biol 1988;33:437–54. https://doi.org/10.1088/0031-9155/33/4/004.
27. Simonot L, Boulenguez P. Generalization of the geometric description of a light beam in radiometry and photometry. J Opt Soc Am A 2013;30:589. https://doi.org/10.1364/josaa.30.000589.
28. Polyanin AD, Zaitsev VF., Moussiaux A. Handbook of first order partial differential equations. London: Taylor & Francics; 2002.
29. Tarasov AP, Rogatkin DA. Scattering specific characteristics of continuous medium for Monte Carlo simulations of light transport in turbid biological tissues. Conf. Proc. - 2019 Radiat. Scatt. Electromagn. Waves, RSEMW 2019, 2019;368–71. https://doi.org/10.1109/RSEMW.2019.8792753.
30. Tarasov AP, Guseva IA, Rogatkin DA. Inaccuracy of the classical Monte Carlo simulation in the general case of 1D turbid biological media. 2016 Int. Conf. Laser Opt. (LO), 2016; S2-24. https://doi.org/10.1109/LO.2016.7549991.
31. Bosschaart N, Edelman GJ, Aalders MC, van Leeuwen TG, Faber D J. A literature review and novel theoretical approach on the optical properties of whole blood. Lasers Med Sci 2014;29:453–79. https://doi.org/ 10.1007/s10103-013-1446-7.
32. Foster MP. The next 50 years of the SI: A review of the opportunities for the e-Science age. Metrologia 2010;47. https://doi.org/10.1088/0026-1394/47/6/R01.